Measurement of the Deformation Potentials for GaAs using Polarized Photoluminescence *

R. A. Mair and R. Prepost
Department of Physics, University of Wisconsin, Madison, WI 53706

E. L. Garwin and T. Maruyama
Stanford Linear Accelerator Center, Stanford, CA 94309

Abstract

The deformation potentials a, b and d for GaAs have been determined from polarized photoluminescence measurements upon a set of epitaxially grown strained GaAs structures possessing varying levels of compressive biaxial lattice strain. X-ray diffraction measurements yield values for the degree of lattice strain while the polarized photoluminescence measurements permit a separate determination of the heavy hole and light hole band energies. Correlation of these data allow determination of the deformation potentials within the context of the Orbital-Strain Hamiltonian.

Measurement of the Deformation Potentials for GaAs using Polarized Photoluminescence

R. A. Mair and R. Prepost

Department of Physics, University of Wisconsin, Madison, Wisconsin 53706

E. L. Garwin and T. Maruyama

Stanford Linear Accelerator Center, Stanford University, Stanford, California 94309

(Nov. 17, 1997)

Abstract

The deformation potentials a, b and d for GaAs have been determined from polarized photoluminescence measurements upon a set of epitaxially grown strained GaAs structures possessing varying levels of compressive biaxial lattice strain. X-ray diffraction measurements yield values for the degree of lattice strain while the polarized photoluminescence measurements permit a separate determination of the heavy hole and light hole band energies. Correlation of these data allow determination of the deformation potentials within the context of the Orbital-Strain Hamiltonian.

Typeset using REVTeX

The development of lattice-mismatched epitaxial growth over the past several years has enhanced the number of material parameters which may be controlled when designing semiconductor structures. The ability to tolerate and incorporate lattice mismatch during epitaxial growth increases the number of pure and alloy semiconductor materials which may be used in multilayer and heterostructure devices. Furthermore, coherent lattice strain may be used to deliberately alter the band structure of a semiconductor by altering the fundamental band gap or splitting electronic states normally degenerate due to crystal symmetry. The parameters which describe the relationship between lattice strain and the electronic band structure are known as deformation potentials, and the accurate measurement of these quantities is important for understanding the band structure of semiconductor devices. Measurements of the deformation potentials for such technologically important materials as GaAs have been previously reported [11]. However there is a significant spread in the reported values. This letter reports on room temperature measurements of the deformation potentials a, b and d for GaAs using a set of samples each consisting of a (001) GaAs layer grown on a strain-inducing GaAsP buffer.

A straightforward and useful method for studying the band structure of a direct bandgap semiconductor, such as GaAs, is through the detection of recombination radiation from optically pumped electrons. Such radiation is referred to as photoluminescence (PL). In a p-type GaAs crystal, electrons optically pumped across the band gap thermalize to the bottom of the conduction band before recombining with valence band holes. Therefore, the resulting PL spectrum is related to the energy dependence and separation of the participating bands. If the polarization states of the optical pump beam and PL are considered, additional information regarding the symmetry of valence and conduction band wave functions may also be obtained.

When a thin epitaxial layer of GaAs is grown on a substrate material possessing a slightly differing lattice constant, the lattice mismatch may be accommodated by a coherent strain within the GaAs layer. Such pseudomorphic growth offers the ability to study GaAs under significant lattice strain ($\sim$1%) without the need of special apparatus designed to apply

external stress. The lattice strain of each sample, measured with standard X-ray diffraction techniques, is correlated with room-temperature polarized PL data in order to determine the deformation potentials. We believe this technique, in which the polarization state of the PL is used to deconvolve PL contributions from the two uppermost strain-split valence bands, to be novel.

The band structure of GaAs, a zinc-blende compound, in the vicinity of the k=0 band gap minimum may be described by the $\vec{k} \cdot \vec{p}$ method introduced by Kane. [1] At the Γ-point, the valence band wave functions have atomic P-like symmetry while the conduction band wave functions are spherically symmetric S states. The heavy hole (V_1) and light hole (V_2) valence bands are degenerate, becoming non-degenerate for non-zero electron momentum. The split-off valence band (V_3) is shifted to lower energy by a value Δ (approximately 340 meV) as a result of the spin-orbit interaction.

The energy dependence and symmetry of the valence band wave functions are affected by lattice strain in a manner described by the orbital-strain Hamiltonian

$$H = -a\epsilon - 3b \times [(L_x^2 - \frac{1}{3}\mathbf{L}^2)\epsilon_{xx} + \text{c.p.}]$$
$$-\frac{6d}{\sqrt{3}}[\{L_x L_y\}\epsilon_{xy} + \text{c.p.}] \quad, \tag{1}$$

where $\epsilon = (\epsilon_{xx} + \epsilon_{yy} + \epsilon_{zz})$, L is the angular momentum operator, a, b, and d are deformation potentials [2], $\{L_x L_y\} = \frac{1}{2}(L_x L_y + L_y L_x)$, and c.p. denotes cyclic permutation with respect to x, y and z. This Hamiltonian is a modification to the non-strained Hamiltonian and is dependent upon the lattice strain tensor ϵ_{ij} and parameterized by the deformation potentials. Using this Hamiltonian, matrix elements within the manifold of Γ point S and P wave functions may be calculated.

The state of strain resulting from lattice-mismatched pseudomorphic growth on a (001) surface is expected to be a biaxial compression or tension with $\epsilon_{xx} = \epsilon_{yy} = (-c_{11}/2c_{12})\epsilon_{zz}$ and $\epsilon_{ij} = 0$ for $i \neq j$ [2]. Here c_{11} and c_{12} are the elastic stiffness constants of the strained material (GaAs), and the relation between the strain along the direction of crystal growth (ϵ_{zz}) and that in the growth plane ($\epsilon_{xx}, \epsilon_{yy}$) is found from the stress-strain relation assuming

that there is no applied stress in the z direction. For such a lattice strain, Eq. 1 yields the following terms for the valence band Γ point wave functions.

$$
\begin{array}{ccc}
V_1 & V_2 & V_3
\end{array}
$$
$$
\begin{pmatrix}
-\delta_h - \delta_s/2 & 0 & 0 \\
0 & -\delta_h + \delta_s/2 & \delta_s/\sqrt{2} \\
0 & \delta_s/\sqrt{2} & -\Delta - \delta_h
\end{pmatrix}
\tag{2}
$$

Here, $\delta_h = a \cdot (2\epsilon_{xx} + \epsilon_{zz})$ and $\delta_s = -2b \cdot (\epsilon_{xx} - \epsilon_{zz})$. The mixing of the V_2 and V_3 states of common m_j in Eq. 2 alters the V_2 band edge energy and must be considered for an accurate calculation of the deformation potentials. For small lattice strain, only terms to first order in strain are considered and the shifted band gaps are given by

$$
E_C - E_{V_1} = E_{gap} + \delta_h + \delta_s/2
\tag{3}
$$

and

$$
E_C - E_{V_2} = E_{gap} + \delta_h - [1 + \delta_s/\Delta] \cdot \delta_s/2
\tag{4}
$$

The term E_{gap} refers to the fundamental band gap of GaAs while E_C refers to the energy of the bottom of the conduction band. Equations 3 and 4 may be used to determine the deformation potentials a and b by relating the measured biaxial strains to the PL peak energies for the set of samples.

When a coherently strained epitaxial layer of GaAs exceeds a critical thickness, the strain is relieved by misfit dislocations. For GaAs and all zinc-blende structures, misfit dislocations develop asymmetrically along the two orthogonal directions [110] and [1$\bar{1}$0] resulting in an anisotropic strain within the plane of the epitaxial layer [3]. The samples used for this study showed partial relaxation and corresponding in-plane shear strains ϵ_{xy}. Such a shear strain introduces Orbital-Strain Hamiltonian terms which depend on d, thus presenting the opportunity to perform a quantitative measurement of this deformation potential. The PL emitted orthogonally from a biaxially compressed GaAs layer should not exhibit any linear polarization component. However, if a small in-plane shear ϵ_{xy} is present, the

4

valence band wave functions will mix in a manner which results in a linear polarization of the photoluminescence. The magnitude of linear polarization is expected to be directly related to the degree of shear strain ϵ_{xy} and parameterized by the deformation potential d. This relationship was discussed and calculated in a paper by Mair et al [4] which described the manifestation of an asymmetry in photoemission quantum efficiency measurements performed while optically pumping with linearly polarized light of varied orientation. The arguments and equations given to describe the quantum efficiency asymmetry are equivalent for the case of linearly polarized PL. As described in reference [4], the maximum possible linear polarization asymmetry corresponds to the condition of transitions involving only V_1 and is given by

$$A_{max} = 2(\delta_1 + \delta_2)\sin 2\phi \ , \tag{5}$$

where δ_1 and δ_2 are linear polarization terms derived from the shear strain induced mixing of V_1 with V_2 and V_3. The equations in reference [4] defining δ_1 and δ_2 neglect the mixing of V_2 and V_3 states seen in Eq. 2 however, and must be appropriately modified for a more accurate calculation of d. The modified equations are

$$\delta_1 = \frac{d \cdot \epsilon_{xy}}{\sqrt{3} \cdot (E_{V_1} - E_{V_2})}(1 - 2\delta_s/\Delta) \tag{6}$$

and

$$\delta_2 = \frac{2d \cdot \epsilon_{xy}}{\sqrt{3} \cdot (E_{V_1} - E_{V_3})}(1 + \delta_s/\Delta) \ , \tag{7}$$

where the V_1 / V_2 mixing terms have been kept only to first order.

The strained samples for the present experiment were grown by the Spire Corporation [5] using Metal-Organic-Chemical-Vapor-Deposition (MOCVD). Each sample consists of a pseudomorphically strained GaAs epitaxial layer grown on a GaAs$_{1-x}$P$_x$ buffer layer (5.0 μm thick), which is itself grown via graded layer technique [6] on a substrate of GaAs vicinally cut approximately 2° from (001). A detailed description of the sample structures is given in an article by Maruyama et al. [7] All the samples show cross-hatch marks on the surface

due to strain relaxation within the $GaAs_{1-x}P_x$ buffer layer. The hatch marks were observed to be predominantly along the $[1\bar{1}0]$ direction and were used to orient the crystal for X-ray diffraction and linearly polarized PL measurements. Table 1 shows the active GaAs layer thickness (t) and phosphorus fraction (x) of the $GaAs_{1-x}P_x$ buffer of the samples used for the experiment.

The lattice structure of the strained GaAs layer for each of the samples was analyzed with a double-crystal x-ray diffractometer. The diffractometer used CuK_α radiation together with a four-crystal Ge(220) monochromator and either a slit with a 2θ acceptance angle of $0.15°$ or a Ge(220) analyzer crystal (triple axis diffractometry). Reciprocal lattice maps were taken to locate the epitaxial GaAs peak relative to the GaAs substrate peak by performing a series of ω-2θ scans, simultaneous rotations of the sample (ω) and detector (2θ), for different ω offsets [8]. Symmetric (004) and asymmetric (224) Bragg reflections were used to measure the lattice constant $a_\perp$ along [001], and two lattice constants $a_{\parallel}^{[110]}$ and $a_{\parallel}^{[1\bar{1}0]}$ along [110] and $[1\bar{1}0]$. The misfit strain along [001] represents the desired tetragonal distortion and is calculated by $\epsilon_{zz} = (a_\perp - a_0)/a_0$, where a_0 is the GaAs lattice constant. Any difference in $a_{\parallel}^{[110]}$ and $a_{\parallel}^{[1\bar{1}0]}$ constitutes an in-plane shear strain which is calculated by $\epsilon_{xy} = (a_{\parallel}^{[110]} - a_{\parallel}^{[1\bar{1}0]})/(a_{\parallel}^{[110]} + a_{\parallel}^{[1\bar{1}0]})$. The measured strain components for the six samples are given in Table 1. The uncertainties quoted for ϵ_{zz} and ϵ_{xy} are based upon the statistical uncertainties in the strained layer X-ray peak positions which were determined by Gaussian fit. Because of the relative degree of difficulty in obtaining the asymmetric Bragg reflections, the shear strain ϵ_{xy} was measured for only two of the six samples.

Each of the samples used in this study was subjected to an etch process in order to remove the GaAs substrate from beneath a small region (~ 1 mm dia.) of the GaAsP buffer and GaAs active layer. Complete removal of the GaAs substrate material was found to be critically necessary in order to obtain PL spectra from the strained GaAs layer without unwanted contributions from the substrate. The procedure used was a light-controlled wet chemical etch technique in which the etch process terminated automatically at the GaAs substrate-GaAsP (graded P content layer) interface. The etch solution was a standard

6

combination of peroxide, water and sulfuric acid. Specific details are described in Ref. [9] and the general concepts of light-controlled etching are described in many articles. [10]

Room temperature PL measurements were obtained for the set of samples under the condition of optical excitation with circularly polarized CW radiation of energy greater than the band gap. A Ti:Sapphire laser pumped with an Argon Ion laser was used as the excitation source. Each sample was pumped at a fixed wavelength in the range of 750 to 780 nm. The typical laser power was approximately 3 mW and the beam was focussed to a spot of ~ 100 μm diameter near the center of the thinned region of a given sample. The samples were pumped from the strained GaAs layer side at approximately 16° from the surface normal, and a cone of PL of half angle 10° emitted along the surface normal was collected. The circular polarization of the excitation laser beam was controlled with a quarter wave retarder–linear polarizer pair. The PL circular polarization was analyzed in a similar manner. The PL wavelength distribution was analyzed with a double spectrometer system equipped with a multichannel diode array detector so that a full PL peak could be acquired at once. All PL spectra were corrected for the spectral response of the spectrometer-detector system by using the acquired spectrum of a calibrated Tungsten ribbon filament lamp.

In order to perform PL polarization measurements, four spectra were acquired under the condition of fixed pump beam power. The spectra were representative of the four possible pump beam–PL analyzer polarization combinations $(\sigma^+/\sigma^+, \sigma^+/\sigma^-,$ etc.). An average spectrum, representative of a zero polarization pump beam was calculated as $I_{avg} = (I_{\sigma^+\sigma^-} + I_{\sigma^-\sigma^+} + I_{\sigma^+\sigma^+} + I_{\sigma^-\sigma^-})$. The PL polarization, P_{PL}, was then determined from $P_{PL} = (I_{\sigma^+\sigma^-} + I_{\sigma^-\sigma^+} - I_{\sigma^+\sigma^+} - I_{\sigma^-\sigma^-})/I_{avg}$. These calculations were performed for the data of each detector array element, thereby generating wavelength dependent intensity and polarization curves.

Fig. 1 shows a PL spectrum and the corresponding polarization curve for sample 1. The polarization is seen to be maximal at the long wavelength (low energy) side of the spectrum and decreasing at shorter wavelengths (larger energy). The structure of the PL polarization curve is assumed to be a consequence of the wavelength dependent ratio of PL contributions

from transitions to each of the two uppermost valence bands. The circular polarization associated with radiative transition from the conduction band to each of the valence bands has magnitude of 100% for a conduction band spin polarization of 100%. However, the circular polarization associated with transition to V_1 is opposite in sign to that associated with recombination to V_2. For the general case of an electron spin polarization S in the conduction band, the PL circular polarization associated with each of the valence bands has magnitude S but is opposite in sign for each valence band. Respective sign values of $+$ and $-$ for the polarization associated with recombination to the V_1 and V_2 valence bands were chosen to be consistent with the experimental geometry and the definition of P_{PL}. The resulting equation describing the wavelength dependence of the PL circular polarization,

$$P_{PL}(\lambda) = S \cdot \frac{(+1)\cdot I_{V_1}(\lambda) + (-1)\cdot I_{V_2}(\lambda)}{I_{V_1}(\lambda) + I_{V_2}(\lambda)} \quad , \tag{8}$$

may be combined with the requirement that $I_{V_1} + I_{V_2} = I_{avg}$ to yield the following equations for the individual PL contributions.

$$I_{V_1}(\lambda) = \frac{1}{2} \cdot [1 + \frac{P_{PL}(\lambda)}{S}] \cdot I_{avg}(\lambda) \tag{9}$$

$$I_{V_2}(\lambda) = \frac{1}{2} \cdot [1 - \frac{P_{PL}(\lambda)}{S}] \cdot I_{avg}(\lambda) \tag{10}$$

Here, S is the average spin polarization of conduction band electrons at the time of recombination and $I_{V_1}(I_{V_2})$ is the PL contribution from the $V_1(V_2)$ valence band.

The PL spectra from the samples were each deconvolved using Eq. 9 and 10. The value of S used for deconvolution was obtained from the maximum of the polarization curve for a given sample because the PL polarization should approach but cannot be larger than the spin polarization of conduction electrons. Determination of the asymptotic maximum of the PL polarization curves is estimated to be accurate to within $\pm 0.5\%$ absolute. The wavelength range for samples 5 and 6 did not extend to a long enough wavelength to observe the full polarization plateau, indicative of the asymptotic approach to maximum possible polarization. Therefore, for samples 5 and 6 the uncertainty for the value of S was correspondingly estimated as $\pm 1.0\%$ absolute which is twice that quoted for samples 1 - 4. An

example of a deconvolved spectrum is shown for sample 1 in Fig. 2. The resultant lineshapes are very similar as expected. Each deconvolved PL curve was fit with a line shape function in order to determine the peak position. For each sample, the peak splitting $(E_{V_1} - E_{V_2})$ and average peak energy $(E_C - \frac{1}{2}(E_{V_1} + E_{V_2}))$ determined from the deconvolutions have a systematic uncertainty related to an uncertainty in the choice of parameters and calibrations and a statistical uncertainty associated with fitting the deconvolved PL spectra. These uncertainties are combined in quadrature to provide a single uncertainty associated with each measured splitting and average energy. The results for the peak splitting and the average peak energy are tabulated in Table 1 along with the values of S used.

The data in Table 1 are used to calculate the deformation potentials a and b for GaAs by fitting the measured values of the peak splitting and the average peak energy to Eq. 11 and 12 respectively. The expected strain dependence of the band splitting is given by the difference of Eq. 3 and 4 and is dependent only on the deformation potential b.

$$E_{V_1} - E_{V_2} = -b \cdot \epsilon_{zz} (\frac{c_{11} + 2c_{12}}{c_{12}})[1 + b \cdot \epsilon_{zz} (\frac{c_{11} + 2c_{12}}{c_{12}})/2\Delta] \tag{11}$$

Similarly, the expected strain dependence of the average band position is given by the average of Eq. 3 and 4, and it is dependent on the deformation potential a with only a very small quadratic dependence on b.

$$E_C - \frac{1}{2}(E_{V_1} + E_{V_2}) = E_{gap} + a \cdot \epsilon_{zz} (\frac{c_{12} - c_{11}}{c_{12}})$$
$$- [b \cdot \epsilon_{zz} (\frac{c_{11} + 2c_{12}}{c_{12}})]^2/4\Delta \tag{12}$$

The relationship $\epsilon_{xx} = \epsilon_{yy} = (-c_{11}/2c_{12})\epsilon_{zz}$ has been used in Eq. 11 and 12 and values for the elastic stiffness constants c_{11} and c_{12} and the spin-orbit splitting Δ inserted. [11] The two PL peak positions for a given sample are assumed to be a valid measurement of the relative band positions because the factors which determine the spectrum shape, i.e. the effective masses of the conduction and valence bands, the Fermi distributions within the conduction and valence bands, and band tailing effects, are expected to be identical or very similar for each spectrum. Furthermore, these factors are expected to have minimal

variation from sample to sample because all were grown by the same vendor and doped to the same nominal level.

Fig. 3 shows the PL peak splitting plotted against lattice strain ϵ_{zz} along with the best fit curve of the form of Eq. 11. The solid line is a best fit of Eq. 11 to the data. From the fit, a value of $b = -2.00 \pm 0.05$ eV is found.

The average PL peak energy plotted against lattice strain ϵ_{zz} is shown in Fig. 4. A best fit of the form of Eq. 12 is also shown yielding a value of $a = -10.19 \pm 0.22$. Here, the value for b obtained from the data in Fig. 3 has been used where needed. The uncertainties quoted for a and b are those associated with the curve fits, both of which have an acceptable χ^2 per degree of freedom.

In order to measure the linear polarization of PL, the polarization analysis system was modified by adding a second quarter wave retarder 'upstream' of the retarder/linear polarizer pair used for the circular polarization analysis. The linear polarization axis ϕ of this analyzer system was then determined by the rotation angle of the 'upstream' retarder and the angle $\phi + 90°$ could accurately be achieved by subsequent indexed rotation of the 'downstream' retarder through 90°. This arrangement was used because it allowed the linear polarization of PL to be analyzed while maintaining a necessarily fixed polarization of PL passed to the spectrometer. The linearly polarized PL asymmetry for any given analyzer angle was defined as

$$P_{lin}(\phi) = [I(\phi) - I(\phi + 90°)]/[I(\phi) + I(\phi + 90°)] \tag{13}$$

where $I(\phi)$ is the PL intensity for a polarization analyzer setting of ϕ and is normalized according to the pump power. The linear polarization was PL wavelength dependent in a manner similar to the PL circular polarization as seen in Fig. 1b, so the ϕ dependent measurement was performed at the PL wavelength range which corresponded to the maximum of the linear polarization. Measurements were performed for several analyzer angle settings and then subsequently repeated after a sample rotation of 90° about the surface normal. False asymmetries introduced by beam steering were then canceled by using one half of the

difference of the values $P_{lin}(\phi)$ obtained for each of the sample orientations.

Fig. 5 shows the PL linear polarization asymmetry as a function of the linear polarization azimuthal angle for the two samples subjected to X-ray measurement of in-plane shear. The crystalline [110] direction was set to nominally $\phi = 45°$ by utilizing the visible cross-hatching on the sample surface, however this alignment was visual only and estimated to be accurate to approximately $\pm 5°$. Also shown in Fig. 5 are $\sin(2\phi)$ curve fits to the data. The amplitude of the curve fit is estimated to be accurate to within $\pm 0.5\%$ absolute as determined from zero-asymmetry checks. For each sample, the curve fit amplitude is taken as the maximum linear polarization asymmetry and used in Eq. 5-7 with the X-ray data and the measured value for b to determine a value for the deformation potential d. Values of -5.04 ± 1.27 for sample 3 and -5.15 ± 0.45 for sample 4 were obtained. These values are combined to yield a result of $d = -5.14\pm0.42$ which is compared with previously published experimental values for d in Table 2.

In conclusion, room temperature photoluminescence spectra obtained from strained layer GaAs structures and subjected to polarization analysis have been used to measure the deformation potentials of GaAs. With this method, the deformation potentials a and b have been measured to an accuracy of better than 3%. Comparisons with previously published measurements are shown in Table 2. The value for b is seen to be in good agreement with previously published values while the value obtained for a is somewhat larger in magnitude than most previous measurements, but is in reasonable agreement with the most accurately quoted value in Table 2. The deformation potential d has also been measured here, although the reported value is less accurate than some previously published values. Only two samples were used for the measurement of d however, and it is likely that the quoted uncertainty can be improved with measurements from additional samples.

REFERENCES

[1] E. O. Kane, J. Phys. Chem. Solids **1**, 249 (1957).

[2] G. Pikus and G. Bir, Sov. Phys.-Solid State **1**, 1502 (1959); H. Hasegawa, Phys. Rev. **129**, 1029 (1963); H. Asai and K. Oe, J. Appl. Phys. **54**, 2052 (1983).

[3] M. S. Abrahams *et al*, Appl. Phys. Lett. **21**, 185 (1972); K. L. Kavanagh *et al*, J. Appl. Phys. **64**, 4843 (1988); M. Grundmann, *et al*, J. Vac. Sci. Technol. **B8**, 751 (1990); A. Bensaada *et al*, J. Crystal Growth **130**, 433 (1993).

[4] R. A. Mair, R. Prepost, H. Tang, E. L. Garwin, T. Maruyama, and G. Mulhollan, Phys. Lett. **A212**, 231 (1996).

[5] Spire Corporation, Bedford, Massachusetts, 01730, USA.

[6] S. M. Vernon *et al*, IEEE Photovoltaic Specialist's Conference **19**, 109 (1987); M. S. Abrahams *et al*, J. Mat. Sci. **4**, 223 (1969).

[7] T. Maruyama, E. L. Garwin, R. Prepost, and G. H. Zapalac, Phys. Rev. **B46**, 4261 (1992).

[8] The reciprocal lattice mapping is described in, for example, P. F. Fewster, Appl. Surf. Sci. **50**, 9 1991.

[9] R. Mair, University of Wisconsin Ph.D. Thesis, 1996, "A Polarized Photoluminescence Study of Strained Layer GaAs Photocathodes", SLAC-Report-488, July 1996.

[10] F. Kuhn-Kuhnenfeld, J. Electrochem. Soc. **119**, 1063 (1972); R. M. Osgood Jr. *et al*, Appl. Phys. Lett. **40**, 391 (1982); D. V. Podlesnik *et al*, Appl. Phys. Lett. **43**, 1083 (1983); D. Moutonnet, Materials Lett. **6** 34 (1987).

[11] *Semiconductors*, New Series III/22a of *Landolt-Börnstein*, edited by O. Madelung (Springer-Verlag, New York, 1987).

[12] J. Feinleib et al., Phys. Rev. **131**, 2070 (1963).

[13] I. Balslev, Solid State Commun. **5**, 315 (1967).

[14] R.N. Bhargava and M.I. Nathan, Phys. Rev. **161**, 695 (1967).

[15] F.H. Pollak and M. Cardona, Phys. Rev. **172**, 816 (1968).

[16] I. Balslev, Phys. Rev. **177**, 1173, (1969).

[17] A. Gavini and M. Cardona, Phys. Rev. **B1**, 672 (1970).

[18] M. Chandrasekhar and F.H. Pollak, Phys. Rev. **B15**, 2127 (1977).

FIGURES

FIG. 1. (a) Room temperature luminescence intensity spectrum (arbitrary units) for sample 1. (b) Corresponding luminescence circular polarization.

FIG. 2. Deconvolved luminescence spectra (arbitrary units) for the two J=3/2 valence bands for sample 1 at room temperature. I_{V_1} refers to the heavy hole transition while I_{V_2} refers to the light hole transition.

FIG. 3. Measured luminescence peak splitting $(E_{V_1} - E_{V_2})$ plotted against the strain along the direction of crystal growth (ϵ_{zz}) for six of the GaAs/GaAs$_{(1-x)}$P$_x$ samples. The solid line is a best fit of Eq. 11 to the data.

FIG. 4. Measured average luminescence peak energy $(E_C - \frac{1}{2}(E_{V_1} + E_{V_2}))$ plotted against the strain along the direction of crystal growth for six of the GaAs/GaAs$_{(1-x)}$P$_x$ samples. The solid line is a best fit of Eq. 12 to the data.

FIG. 5. Linear polarized luminescence asymmetry for samples 3 (a) and 4 (b) plotted against the angle ϕ measured relative to the in-plane crystalline axes of the samples. The asymmetry is defined by Eq. 13. The solid lines represent the best fits to the data.
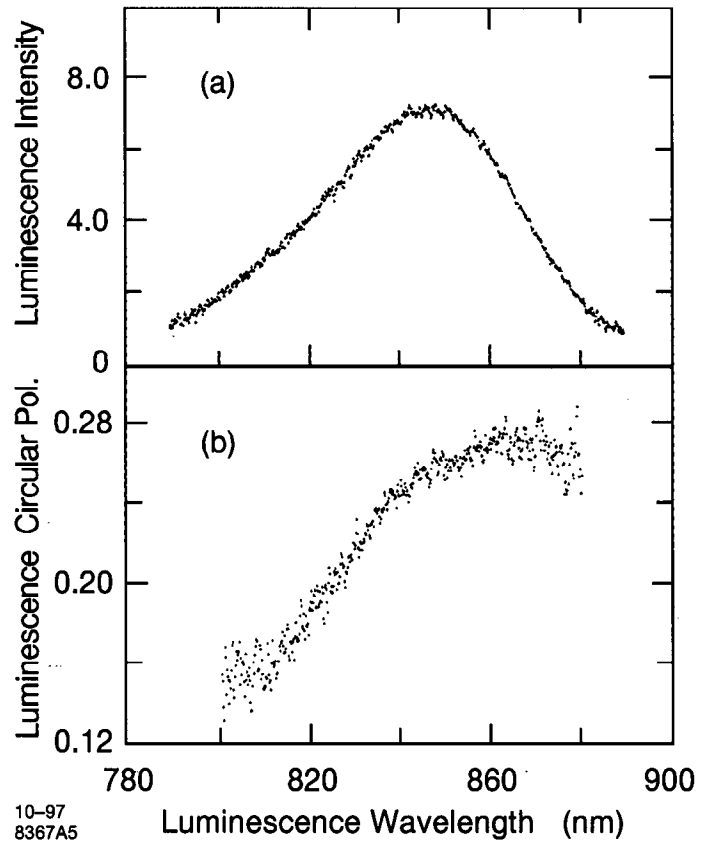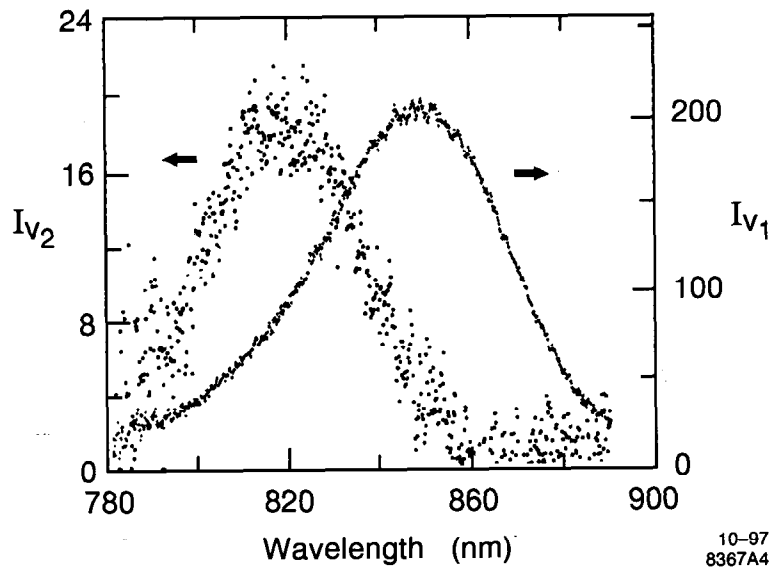
TABLES

TABLE I. Properties of the six samples described in the text. The thickness of the strained epitaxial layer is denoted by t, and x is the P fraction in the $GaAs_{1-x}P_x$ buffer layer. The strain components ϵ_{zz} and ϵ_{xy} refer to the strains along the direction of crystal growth and in the plane of the surface respectively. S is the average spin polarization of conduction band electrons at the time of recombination. The values for $(E_{V_1} - E_{V_2})$ and $(E_C - \frac{1}{2}(E_{V_1} + E_{V_2}))$ are measured quantities used in the determination of the deformation potentials.
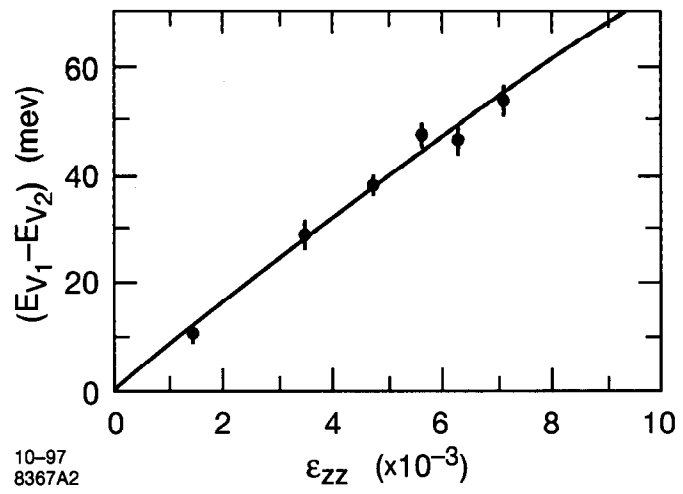
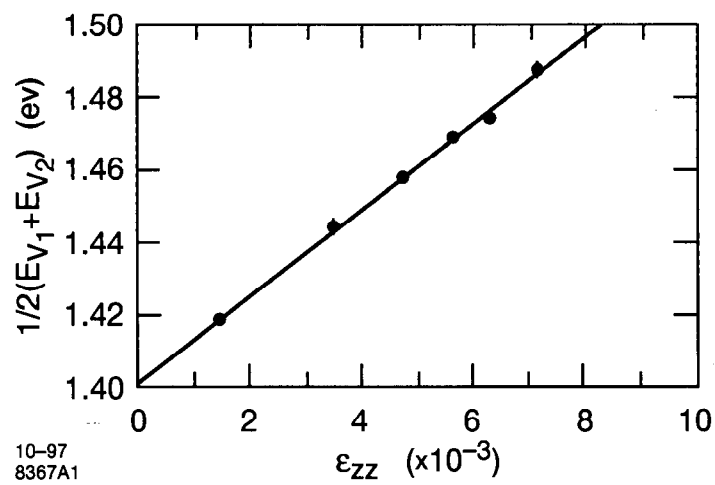| Sample	1	2	3	4	5	6
t (nm)	100	100	100	200	300	500
x	0.288	0.261	0.200	0.247	0.231	0.233
$\epsilon_{zz}(\times 10^{-3})$	7.14± 0.07	6.29± 0.07	4.73± 0.07	5.63± 0.07	3.48± 0.07	1.44± 0.07
$\epsilon_{xy}(\times 10^{-4})$	$\cdots$	$\cdots$	−1.50± 0.30	−4.74± 0.30	$\cdots$	$\cdots$
S	0.266± 0.005	0.292± 0.005	0.316± 0.005	0.287± 0.005	0.320± .010	0.350± .010
$(E_{V_1} - E_{V_2})$ (meV)	53.4± 2.5	46.2± 2.4	37.9± 1.7	47.2± 2.0	28.6± 2.7	10.4± 1.6
$(E_C - \frac{1}{2}(E_{V_1} + E_{V_2}))$ (meV)	1487.9± 1.4	1474.6± 1.4	1458.2± 1.0	1469.4± 1.2	1444.9± 1.5	1418.7± 1.0

TABLE II. Comparison of deformation potential values for GaAs with previously published measurements.
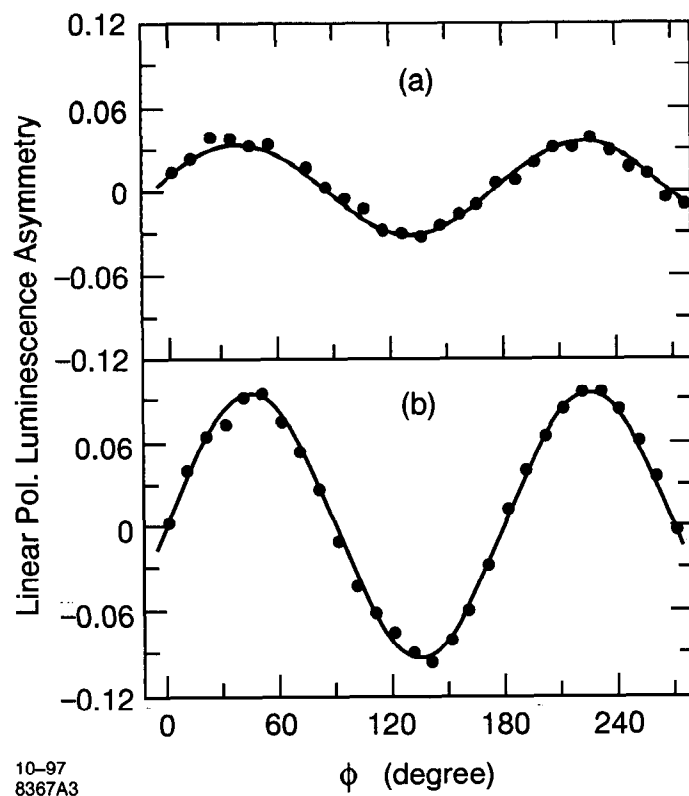
Reference	a (eV)	b (eV)	d (eV)
Present Work	−10.19± 0.22	−2.00± 0.05	−5.14± 0.42
[11]	−9.77± 0.08	$\cdots$	$\cdots$
[12]	−8.7± 0.4	−2.1± 0.1	−6.5± 0.3
[13]	$\cdots$	−1.7± 0.2	−4.4± 0.5
[14]	$\cdots$	−2.0± 0.1	−5.4± 0.3
[15]	$\cdots$	−2.0± 0.2	−6.0± 0.4
[16]	$\cdots$	−2.0± 0.2	−5.3± 0.4
[17]	$\cdots$	−1.75± 0.3	−5.5± 1.1
[18]	−8.93± 0.9	−1.76± 0.1	−4.59± 0.25
[18]	−8.14± 0.8	−1.66± 0.1	−4.52± 0.25